Article

Exact Mathematical Solution for Maximum Transient Offtracking Calculation of a Single-Unit Vehicle Negotiating Circular Curves

Vladan Ilić * [ID], Miloš Lukić [ID], Dejan Gavran, Sanja Fric, Filip Trpčevski, Stefan Vranjevac [ID] and Nikola Milovanović [ID]

Faculty of Civil Engineering, University of Belgrade, 11120 Belgrade, Serbia; mlukic@grf.bg.ac.rs (M.L.); gavran@eunet.rs (D.G.); sfric@grf.bg.ac.rs (S.F.); ftrpcevski@grf.bg.ac.rs (F.T.); svranjevac@grf.bg.ac.rs (S.V.); nmilovanovic@grf.bg.ac.rs (N.M.)

* Correspondence: vilic@grf.bg.ac.rs

Featured Application: The best use of this paper is for the revision of the worldwide used ICAO calculation procedure for fillet design elements at airports. Also, the developed calculation method for maximum transient offtracking calculation can be used for more accurate positioning of single-unit autonomous road vehicles negotiating circular curves.

Abstract: The low-speed turning maneuverability of vehicles is closely related to a well-known offtracking phenomenon which occurs when the rear wheels of a turning vehicle deviate towards the inside of a horizontal curve. Although numerous mathematical models and computer programs for vehicle swept path analysis have been developed in the past, only a few of them can calculate the maximum transient offtracking of a turning vehicle, yet with limited accuracy. The authors were motivated by this fact to find a new mathematical solution for maximum transient offtracking calculation of a single-unit vehicle when negotiating circular curves. In the first stage, a transcendental equation defining vehicle maximum transient offtracking position is derived and numerically solved by Python 3.10.12. In the second stage, the polynomial regression model predicting accurate numerical solutions of the transcendental equation with the desired level of accuracy was developed and tested. The new calculation method is simple enough to simply take the vehicle datum length, circular curve radii, and turn angle, while instantly producing the maximum transient offtracking value, without the need to draw any of the vehicle movement trajectories.

Keywords: road design; low-speed offtracking; maximum transient offtracking; vehicle movement; ICAO; transcendental equation; numerical solution; Python; polynomial regression model

1. Introduction

When a vehicle turns, particularly trucks or other long wheelbase vehicles, the rear wheels deviate inside the path traced by the front wheels. The trailing axles of a turning vehicle increasingly deviate towards the curve center, until the rear axle wheels finally reach the maximum steady-state offset from the steering alignment path. This phenomenon is well known in transportation engineering as low-speed offtracking [1–3]. In contrast to this phenomenon, high-speed offtracking introduces movements of trailing vehicle axels outward the curve center due to the lateral acceleration of the vehicle as it traverses a horizontal curve at high speeds [4,5]. In addition to the vehicle wheelbase length, road geometry parameters, such as the turn radius and turn angle, dominantly influence offtracking intensity [6]. In general, two different states of low-speed offtracking exist: steady-state offtracking and active transient state offtracking.

According to the authors of [7], steady-state offtracking is not normally reached before covering turn angle of 270°. This means that particular vehicle will reach steady-state offtracking only after covering a constant radius curve with a turn angle greater

than 270°. The most widely accepted procedure for steady-state offtracking calculation is the traditional "sum of squares" method originally developed by the Western Highway Institute (WHI), and published in 1970 [8], and the letter repeatedly revised by the Society of Automobile Engineers—SAE International [9,10].

Since roadway edges, especially in intersection zones, are usually designed with relatively small radii and with turn angles in the order of 90°, the potential application of steady-state offtracking calculation methods is quite limited, if not questionable, in practice. When a vehicle performs a sharp turn like this one, it remains in an active transient offtracking state. Hence, the question how to accurately calculate the maximum offtracking value for a vehicle if an active transient offtracking state arises.

Perhaps the most acute problem related to the lack of accurate transient offtracking calculation comes from the field of airport design. The official ICAO procedure for taxiway fillet design [11] assumes that the maximum offtracking is reached when the aircraft datum point (usually the cockpit) reaches the end of the taxiway lead arc, which is incorrect. The consequence is an insufficient pavement width in taxiway turns. Even in standard cases (turn angle of 90° and radii of 50 m), the magnitude of error is in the range of 0.30–0.75 m. In less common dispositions, when larger aircrafts, i.e., the Airbus A380, negotiate sharp turns, the error exceeds an enormous 4.3 m!

Also, the lateral positioning of autonomous vehicles in relation to the geometry of roadway edges demands efficient transient offtracking assessment in order to safely guide vehicle through the crossroad [12–14]. This is especially critical in the case of an articulated autonomous vehicle such as a semi-tractor trailer [15,16].

In past decades, numerous mathematical and numerical models for setting vehicles' movement trajectories, while negotiating different steering path alignment configurations, have been developed and tested in the field [17–23]. Additionally, commercial computer programs for the simulation of vehicle movements and vehicle swept path analysis, such as the Auto CAD Vehicle Tracking 2024 and Transoft AutoTURN 12.0.0, have become indispensable tools for civil engineers and other specialists involved in intersection and roundabout design [24,25]. Recently, extensive analyses, addressing the accuracy of the available numerical models and commercial software applications for setting vehicle movement trajectories, were conducted in a Ph.D. thesis [26]. However, amongst all of the addressed mathematical and numerical models, only a few of them offered a solution for the calculation of the exact vehicle position where the maximum active transient offtracking is reached [7,27]. This position indicates the exact cross section where the width of the pavement is at its maximum. The distance between the inner edge of the pavement and the steering path, at this very location, is of crucial importance when it comes to some elements of the crossroads [28,29]. For example, in the most standards and design practices [1,30], the usual width of the right-turn channel passing behind the triangular isle is 4.5–5.5 m. Though such a channel is slightly tapered (getting narrower towards its end), its net width is constant, as measured between the marking lane on the left and the curb on its right side. This particular net width comes directly from the maximum transient offtracking. Also, when it comes to the spiral ramps in multilevel garages (180° turns), their width is a direct consequence of the maximum transient offtracking.

Nowadays, as demonstrated in [26], their efficiency and accuracy are not enough for road infrastructure design purposes, especially for autonomous vehicle positioning in horizontal curves. For example, the results of the maximum transient offtracking calculation in Lawrence's mathematical model for low-speed offtracking [27] are generated by the computer in a form of a graph. Before plotting the graph, equations determining the maximum transient offtracking vehicle position were numerically solved by the computer program. The graph shows the maximum offtracking for turn angles of up to 300° and various wheelbase/turn radius ratios. The graph is simple and suitable for everyday use, but the mathematical apparatus underlining the graph is not available to the user. In other words, the user cannot check the validity of the maximum transient offtracking graphically read from the diagram. The computation workload of Woodrooffe's method [7]

is equivalent to ICAO's [11]. The method relies on the deployment of an "equivalent base", acting as a virtual base of an entire multibody vehicle assembly. Woodrooffe's procedure retrieves the maximum transient offtracking value, but with the error of 0.06–0.10 m in lateral terms and more than 1.2 m in longitudinal terms, as proven in [26]. On the other hand, commercially available software tools for vehicle swept path analysis based on CAD platform require from the user to draw guideline first, and then based on its shape and generated swept path width, determine the maximum transient offtracking for a selected design vehicle [31].

The aforementioned deficiencies were the key motivation for the authors of this paper to develop an exact mathematical solution for the maximum transient offtracking calculation in sharp turns. In fact, the primary aim was to develop mathematical formulas which will calculate accurately single-unit vehicle position where the maximum transient offtracking is reached. The new calculation method will eliminate the need to perform the vehicle movement simulations first and draw any of the vehicle movement trajectories, before determining the maximum transient offtracking value. Thus, by avoiding unnecessary procedures, calculation method presented herein is simple enough just to enter the vehicle datum length *d*, circular radii *R* and turn angle, and instantly produces the maximum transient offtracking value, including the vehicle position where this maximum transient offtracking is reached.

The sections in the paper are structured in the following order. In Section 2, mathematical definition of the problem and necessary parameters are presented, while in Section 3, mathematical solution of the problem is given. In Section 4 the accuracy of developed calculation method based on adopted regression model was evaluated and discussed. The last, Section 5, contains conclusions and future research plan to further improve application of the presented calculation method.

2. Problem Statement and Input Parameters

The International Civil Aviation Organization (ICAO) has its own mathematical model for the offtracking calculation of the main undercarriage center of the aircraft [11]. Based on this mathematical model, fillets at taxiways turns and intersections are designed. The same model applies to movement of an aircraft leaving its parking position on an apron or maneuvering on a holding bay. Basic terms and symbols related to aircraft kinematic model, taxiway and fillet design are displayed in Figures 1 and 2.

In Figure 2b the path of the aircraft main undercarriage center (*U*), while the aircraft cockpit negotiates circular curve, is shown. Actually, the shortest distance between the circular curve denoting aircraft's cockpit guideline and the path of the main undercarriage center represents offtracking. The position of aircraft while its datum point, or cockpit, (*S*) follows an arc of a circular radii *R* can be determined based on the arc length expressed by its central angle θ_S and the steering angle β. According to ICAO mathematical model [11], the steering angle β between the tangent on the arc in the datum point (*S*) and the aircraft longitudinal axis is calculated as follows:

$$tan\left(\frac{\beta}{2}\right) = \frac{1 - e^{K\theta_S}}{X - K - X \cdot e^{K\theta_S} - K \cdot e^{K\theta_S}}$$ (1)

where the angle θ_S should be entered in radians.

As the result of the calculation, Equation (1) returns the value of the steering angle β also expressed in radians. It should be noted that Equation (1) was derived assuming that $R > d$, where *d* is the aircraft datum length in meters (Figure 1b). In addition to the taxiway center line, which is followed by the airplane cockpit during turning maneuver, the example of two fillets, each composing of an arc of a circle and two tangents, can be seen in Figure 2c.

The parameters X and K used in Equation (1), respectively, refer to the following:

$$X = \frac{R}{d} \tag{2}$$

$$K = \sqrt{X^2 - 1} \tag{3}$$

The maximum steering angle β_{max} is achieved when the aircraft datum point (S) reaches the end of a circular arc (Figure 3). However, according to the authors of mathematical models for transient offtracking calculation [7,27], the maximum transient offtracking of the main undercarriage center is not reached at the same point as the angle β_{max} (at the end of arc), but some distance beyond the end of the arc (Figure 4). Thus, as will be demonstrated later, the ICAO's assumption that the aircraft main undercarriage center reaches the maximum transient offtracking in the same position in which the β_{max} is achieved causes a significant error.
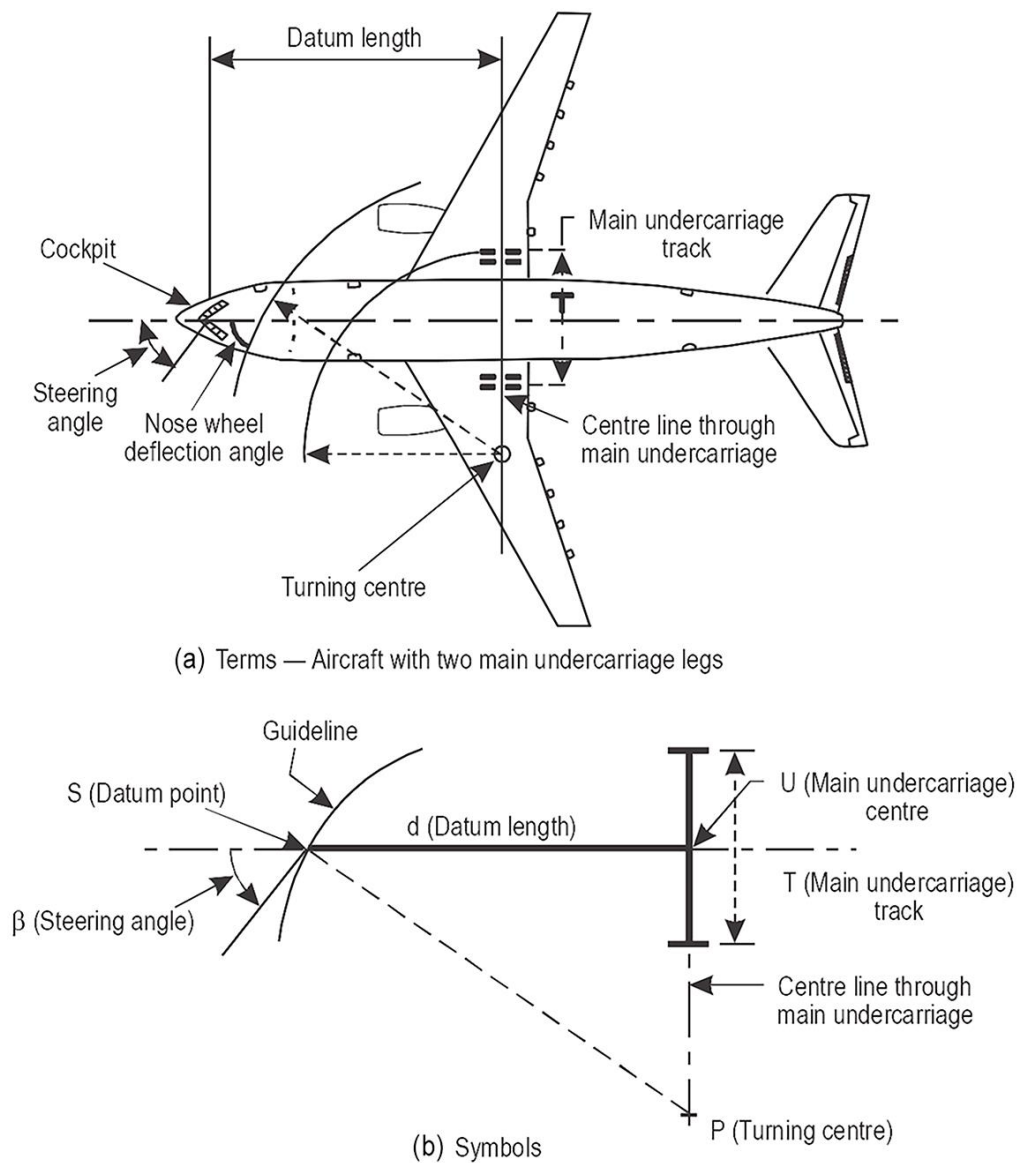

Figure 1. Terms and symbols related to the aircraft kinematic model (adapted from [11]).
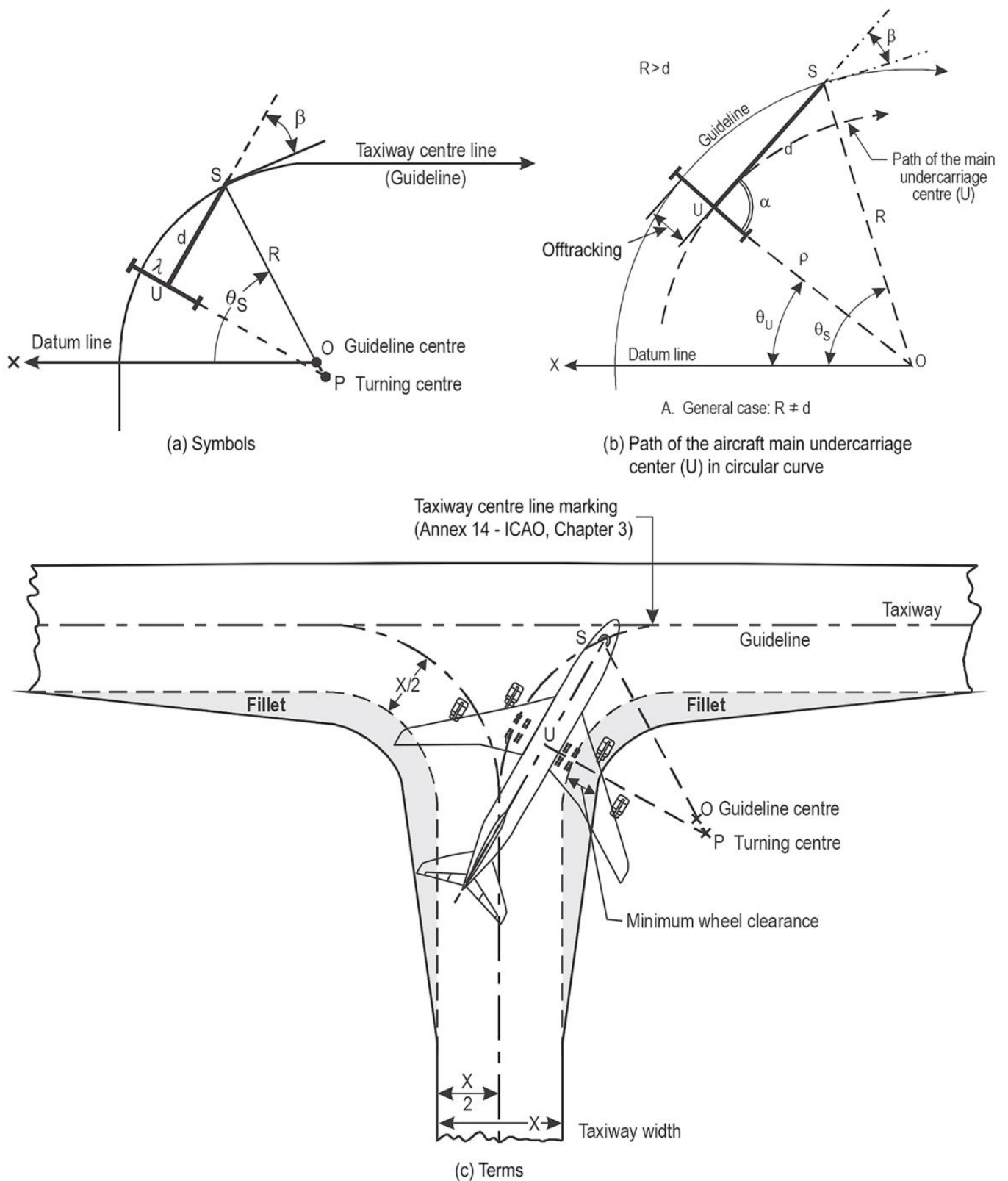
Figure 2. Terms and symbols related to taxiway and fillet design (adapted from [11]).
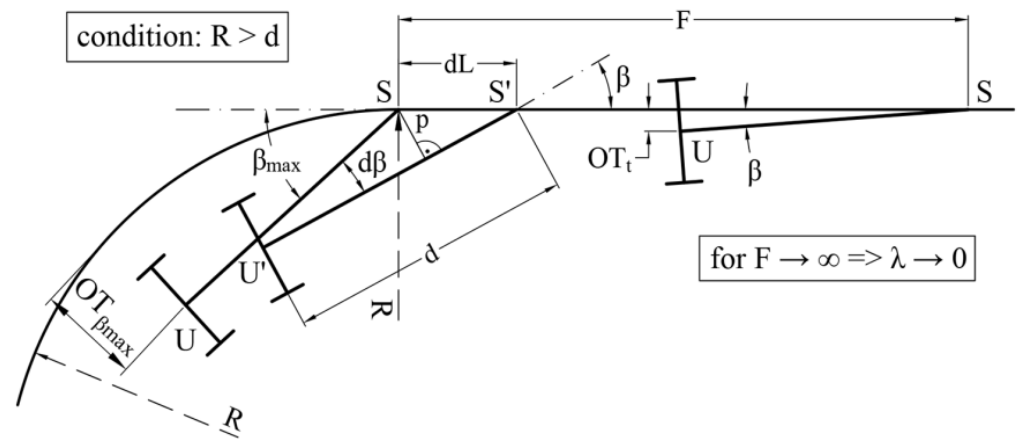
Figure 3. Offtracking of the aircraft main undercarriage center (*U*) when its datum point (*S*) follows a straight exit guideline (adapted from [11]).
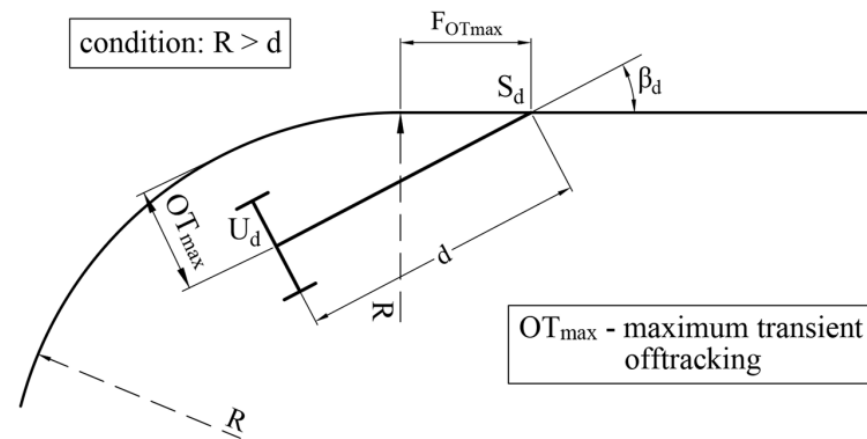
Figure 4. Aircraft position where its main undercarriage center (*U*) reaches the maximum transient offtracking *OTmax*.

While the datum point (*S*) follows a straight guideline coinciding with the arc exit tangent, the steering angle *β* progressively decreases and the aircraft main undercarriage center (*U*) follows a tractrix (Figure 3). As defined in the ICAO mathematical model [11], the steering angle *β* is calculated as a function of the distance *F* which the datum point (*S*) has covered along the straight exit tangent:

$$ ln\left(tan\left(\frac{\beta}{2} \right) \right) = ln\left(tan\left(\frac{\beta_{max}}{2} \right) \right) - \frac{F}{d} \tag{4} $$

where *β_{max}* represents, again, the maximum steering angle at the end of an arc, and *d* is the aircraft datum length. In the last 60 years the ICAO mathematical model has been used for fillet designs at international airports by civil aviation authorities all over the world, and the accuracy of Equations (1) and (4) is unquestionable.

By applying simple transformation, Equation (4) can be written in a more convenient form:

$$ F = d \cdot ln\left[\frac{tan\left(\frac{\beta_{max}}{2} \right)}{tan\left(\frac{\beta}{2} \right)} \right] \tag{5} $$

It is important to emphasize that all the formulas in the ICAO mathematical model, derived for the calculation of the aircraft undercarriage offtracking, can also be applied to the calculation of offtracking for a single-unit vehicle. In contrast to the aircraft undercarriage, where the datum point was located exactly in the center of the aircraft cockpit, the datum point on the datum length of the single-unit vehicle is usually defined as the most prominent point in the center line of the vehicle front part, i.e., the point in the middle of the vehicle front bumper (Figure 5).

Example of single-unit vehicle: city bus
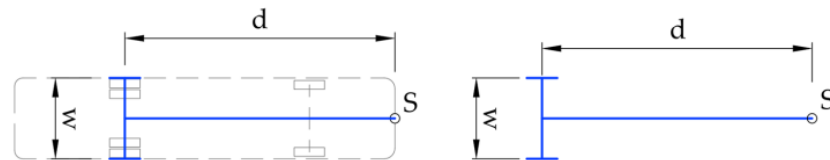
d - datum length (coinciding with the vehicle center line)
S - datum point (in the middle of the vehicle front bumper)
w - vehicle track width

Figure 5. Terms and symbols related to the kinematic model of a single-unit vehicle.

Looking at Figure 4, and based on the previously described formulas from the ICAO mathematical model, the calculation of the exact aircraft position where its main undercarriage center (U) reaches the maximum transient offtracking OT_{max} arises as a key problem that will be addressed in this paper. This particular aircraft position is determined by two parameters: the distance F_{OTmax} which the datum point (S) has covered along the straight exit tangent, and the steering angle β_d between the longitudinal aircraft axis and the exit tangent direction. Therefore, in the maximum transient offtracking position, based on the previous Equation (5), a new equation is established:

$$F_{OTmax} = d \cdot ln\left[\frac{tan\left(\frac{\beta_{max}}{2}\right)}{tan\left(\frac{\beta_d}{2}\right)}\right] \tag{6}$$

Since there are two unknown variables, distance F_{OTmax} and the angle β_d, basic mathematical logic requires forming a system composed of two different equations in order to calculate these two variables. As Equation (6) applies to all positions of the aircraft when its datum point follows the exit tangent, for the second equation of the system it is necessary to find another reliable relation between the distance F_{OTmax} and the angle β_d that would be valid only in the position where the maximum transient offtracking is reached.

The required additional relation between the distance F_{OTmax} and the angle β_d is obtained from the study [27] focused on the development of a mathematical model for transient offtracking calculation. This study proved that the maximum transient offtracking of a single-unit vehicle occurs when the direction of the motion of the rear axle (vector $\vec{m}$) is parallel to the tangent to the steering path (guideline). The geometry describing this case is shown in Figure 6. In other words, only in the maximum transient offtracking position is the direction of the vector $\vec{m}$ perpendicular to the line passing through the center of the rear axle (U) and the circular arc center C. Only in this particular position is the distance of the vehicle datum point (S) from the beginning of the exit tangent F_d equal to the unknown distance F_{OTmax}:

$$F_d = F_{OT_{max}} \tag{7}$$
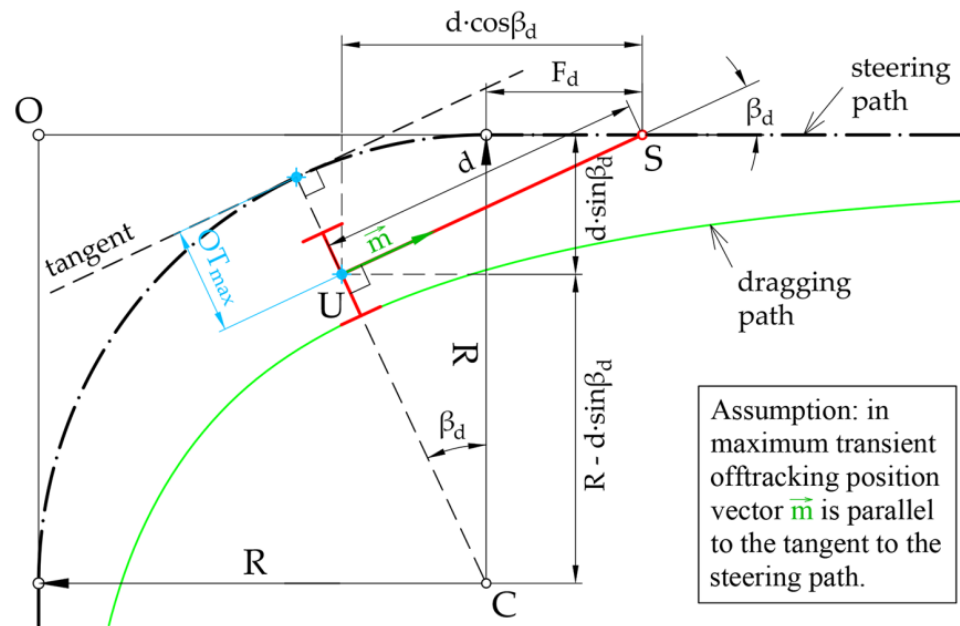
Figure 6. Geometry describing the unique position of a single-unit vehicle when the maximum transient offtracking is achieved.

Using simple geometric relations retrieved from Figure 6 and the previous identity in Equation (7), the following equation is established:

$$d \cdot cos\beta_d - F_d = (R - d \cdot sin\beta_d) \cdot tg\beta_d \tag{8}$$

where the required distance F_d can further be expressed as follows:

$$F_d = d \cdot cos\beta_d - (R - d \cdot sin\beta_d) \cdot tg\beta_d \tag{9}$$

Since the required angle β_d varies in the range $0 < \beta_d < \beta_{max}$, and β_{max} is always $\beta_{max} < 90°$, both sides of Equation (9) can be multiplied by $cos\beta_d$. Namely, as it is well known from trigonometry that $cos\alpha$ always has positive values in the angle range $0 < \alpha < 90°$, Equation (9) becomes

$$F_d \cdot cos\beta_d = d \cdot cos^2\beta_d - R \cdot sin\beta_d + d \cdot sin\beta_d \cdot sin\beta_d \tag{10}$$

$$F_d \cdot cos\beta_d = d \cdot \left(cos^2\beta_d + sin^2\beta^d\right) - R \cdot sin\beta_d \tag{11}$$

Bearing in mind the basic trigonometry identity $sin^2_{\beta_d} + cos^2_{\beta_d} = 1$, Equation (11) eventually becomes the following:

$$F_d = \frac{d - R \cdot sin\beta_d}{cos\beta_d} \tag{12}$$

Now, both equations of the system that should be solved in order to calculate the required variables F_d and β_d which determine the maximum transient offtracking position are known:

$$F_d = d \cdot ln\left[\frac{tan\left(\frac{\beta_{max}}{2}\right)}{tan\left(\frac{\beta_d}{2}\right)}\right]$$

$$F_d = \frac{d - R \cdot sin\beta_d}{cos\beta_d} \tag{13}$$

3. Mathematical Solution of the Problem

3.1. Transformation and Solving the Established Equation System

The angle β_d could be calculated by taking the right sides from Equation (13) as equal:

$$\frac{d - R \cdot sin\beta_d}{cos\beta_d} = d \cdot ln\left[\frac{tan\left(\frac{\beta_{max}}{2}\right)}{tan\left(\frac{\beta_d}{2}\right)}\right] \tag{14}$$

Both sides of the newly formed Equation (14) can be divided by the datum length d, and then transformed:

$$d \cdot \frac{1 - \frac{R}{d} \cdot sin\beta_d}{cos\beta_d} = d \cdot ln\left[\frac{tan\left(\frac{\beta_{max}}{2}\right)}{tan\left(\frac{\beta_d}{2}\right)}\right] \tag{15}$$

$$\frac{1}{cos\beta_d} - \frac{R}{d} \cdot \frac{sin\beta_d}{cos\beta_d} = ln\left[\frac{tan\left(\frac{\beta_{max}}{2}\right)}{tan\left(\frac{\beta_d}{2}\right)}\right] \tag{16}$$

$$\frac{1}{cos\beta_d} - \frac{R}{d} \cdot tg\beta_d = ln\left[\frac{tan\left(\frac{\beta_{max}}{2}\right)}{tan\left(\frac{\beta_d}{2}\right)}\right] \tag{17}$$

The maximum steering angle β_{max} can be calculated applying Equation (1) from the ICAO mathematical model, described in the previous section:

$$tan\left(\frac{\beta_{max}}{2}\right) = \frac{1 - e^{K\theta_S}}{X - K - X \cdot e^{K\theta_S} - K \cdot e^{K\theta_S}} \tag{18}$$

Considering Equations (2) and (3), the angle β_{max} directly depends on the steering path circular radii R, the datum length d, and the turning angle θ_s which are constant when performing the turning maneuver. In accordance with that, the angle β_{max} also represents a constant value. Therefore, in order to facilitate the solving of Equation (17), the constant c is introduced:

$$c = tan\left(\frac{\beta_{max}}{2}\right) \tag{19}$$

To further simplify the Equation (17), the following trigonometry half-angle identities are used:

$$cos\beta_d = \frac{1 - tg^2\left(\frac{\beta_d}{2}\right)}{1 + tg^2\left(\frac{\beta_d}{2}\right)} \tag{20}$$

$$tg\beta_d = \frac{2 \cdot tg\left(\frac{\beta_d}{2}\right)}{1 - tg^2\left(\frac{\beta_d}{2}\right)} \tag{21}$$

and Equation (17) takes the following form:

$$\frac{1}{\frac{1 - tg^2\left(\frac{\beta_d}{2}\right)}{1 + tg^2\left(\frac{\beta_d}{2}\right)}} - \frac{R}{d} \cdot tg\beta_d = ln\left[\frac{c}{tan\left(\frac{\beta_d}{2}\right)}\right] \tag{22}$$

$$\frac{1 + tg^2\left(\frac{\beta_d}{2}\right)}{1 - tg^2\left(\frac{\beta_d}{2}\right)} - \frac{R}{d} \cdot \frac{2 \cdot tg\left(\frac{\beta_d}{2}\right)}{1 - tg^2\left(\frac{\beta_d}{2}\right)} = ln\left[\frac{c}{tan\left(\frac{\beta_d}{2}\right)}\right] \tag{23}$$

Finally, by introducing the substitution $t = tg\left(\frac{\beta_d}{2}\right)$, Equation (23) is transformed into the following:

$$\frac{1+t^2}{1-t^2} - \frac{R}{d} \cdot \frac{2 \cdot t}{1-t^2} = ln\left(\frac{c}{t}\right) \tag{24}$$

$$\boxed{ln\left(\frac{c}{t}\right) = \frac{1 - 2 \cdot \frac{R}{d} \cdot t + t^2}{1 - t^2}} \tag{25}$$

The last equation represents the most important contribution to the exact mathematical solution of the addressed problem. Its solution first returns the value of the substitution t, and then consequently the required parameters F_d and β_d which precisely determine the maximum transient offtracking vehicle position.

Nevertheless, Equation (25) belongs to the group of transcendental equations that cannot be solved by classic algebraic methods alone and often require the application of various numerical techniques, i.e., the Newton–Raphson method, bisection method, secant method, regula falsi methods, etc. Additionally, these numerical methods are useful for approximating the equation solution to any desired degree of accuracy [32].

The only unknown variable in Equation (25) is the substitution t which refers to the angle between the arc exit tangent and the vehicle's longitudinal axis. Given that the required steering angle β_d varies in the range $0 < \beta_d < \beta_{max}$, then the calculated values of the previously introduced substitution $t = tg\left(\frac{\beta_d}{2}\right)$ can vary only in the following range:

$$0 < t < tg\left(\frac{\beta_{max}}{2}\right) \tag{26}$$

Considering that Equation (19) has introduced the constant c, the inequality (26) can be written as follows:

$$0 < t < c \tag{27}$$

As it has already been stated that $\beta_{max} < 90°$ and $tg\left(\frac{90°}{2}\right) = 1$, the last inequality eventually takes the following form:

$$0 < t < 1 \tag{28}$$

Thus, in addition to the condition $R > d$ formerly imposed by the ICAO, all values of the substitution t obtained from the numerical solution of Equation (25) should be in the $0 < t < 1$ range.

3.2. Numerical Solution of Derived Transcedental Equation

For the numerical solution of the transcendental Equation (25), a new Python script following the algorithm flow chart displayed in Figure 7 is written. At first, the input dataset is generated by varying the turn angles θ_S, circular arc radii R, and vehicle datum lengths d. For each of the 30 analyzed turn angles θ_S varying from 30° to 180°, and circular radii to datum length ratios R/d in the range $1.0101 < R/d < 5.0$, unknown values of the substitution t are calculated. The used ratios R/d are limited to within a specified range because other combinations of the designed vehicles' datum lengths and radius of the horizontal curves negotiated by these vehicles are not common in road design practice.

In line with the assumptions in the previous section of the paper, only the calculated values of the substitution t that meet the condition $0 < t < 1$ are plotted as results. A total of 26,400 different combinations of turning angles and ratios R/d from the input dataset are addressed. Selected parameters in the input dataset and the obtained results of the calculation are shown condensed in Table 1.
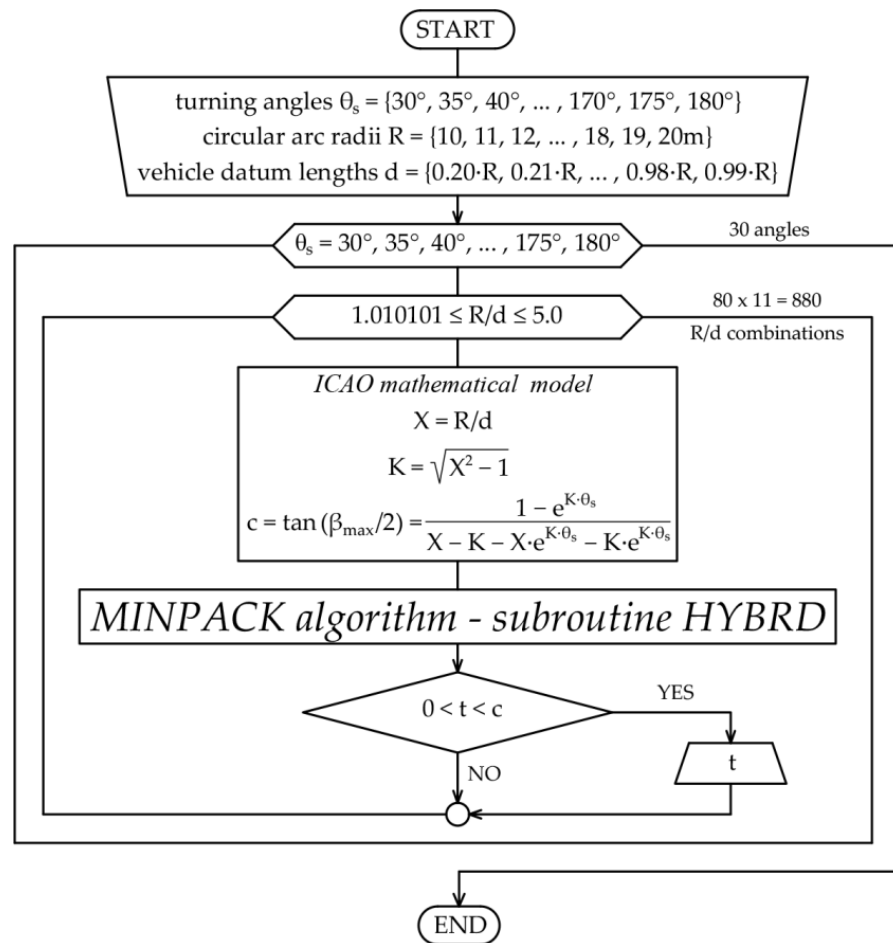
Figure 7. Flow chart of the algorithm used for the numerical solution of a transcendental equation.

Table 1. Input dataset for numerical calculation of transcendental equation and obtained results.

	Input Parameters								Results	
No *	θ_S [°]	R [m]	d [m]	R/d	K	$e^{K\theta s}$	c	β_{max} [°]	t	β_d [°]
1	30.00	10.00	2.00	5.000000	4.898979	13.001954	0.093324	10.6633	0.066106	7.5642
2	30.00	10.00	2.10	4.761905	4.655721	11.447024	0.097003	11.0811	0.067365	7.7078
3	30.00	10.00	2.20	4.545455	4.434090	10.192827	0.100561	11.4848	0.068529	7.8406
4	30.00	10.00	2.30	4.347826	4.231264	9.165848	0.104000	11.8748	0.069609	7.9637
5	30.00	10.00	2.40	4.166667	4.044887	8.313643	0.107323	12.2514	0.070612	8.0782
6	30.00	10.00	2.50	4.000000	3.872983	7.598033	0.110534	12.6151	0.071547	8.1848
7	30.00	10.00	2.60	3.846154	3.713879	6.990714	0.113638	12.9663	0.072420	8.2843
8	30.00	10.00	2.70	3.703704	3.566149	6.470358	0.116636	13.3054	0.073236	8.3773
9	30.00	10.00	2.80	3.571429	3.428571	6.020653	0.119534	13.6330	0.074001	8.4645
10	30.00	10.00	2.90	3.448276	3.300092	5.628956	0.122336	13.9493	0.074720	8.5464
11	30.00	10.00	3.00	3.333333	3.179797	5.285346	0.125044	14.2550	0.075395	8.6233
12	30.00	10.00	3.10	3.225806	3.066892	4.981948	0.127663	14.5504	0.076031	8.6958
13	30.00	10.00	3.20	3.125000	2.960680	4.712452	0.130197	14.8360	0.076632	8.7642
14	30.00	10.00	3.30	3.030303	2.860548	4.471749	0.132648	15.1121	0.077199	8.8288
15	30.00	10.00	3.40	2.941176	2.765957	4.255668	0.135020	15.3792	0.077736	8.8900
16	30.00	10.00	3.50	2.857143	2.676428	4.060777	0.137317	15.6376	0.078244	8.9479
17	30.00	10.00	3.60	2.777778	2.591534	3.884227	0.139541	15.8876	0.078727	9.0029

Table 1. *Cont.*

	Input Parameters								Results	
No *	θ_S [°]	R [m]	d [m]	R/d	K	$e^{K\theta s}$	c	β_{max} [°]	t	β_d [°]
•	•	•	•	•	•	•	•	•	•	•
•	•	•	•	•	•	•	•	•	•	•
•	•	•	•	•	•	•	•	•	•	•
26,384	180.00	20.00	16.60	1.204819	0.672004	8.257840	0.484965	51.7435	0.357094	39.3026
26,385	180.00	20.00	16.80	1.190476	0.645936	7.608518	0.492151	52.4083	0.359695	39.5668
26,386	180.00	20.00	17.00	1.176471	0.619744	7.007523	0.499366	53.0720	0.362259	39.8268
26,387	180.00	20.00	17.20	1.162791	0.593365	6.450203	0.506612	53.7347	0.364787	40.0826
26,388	180.00	20.00	17.40	1.149425	0.566726	5.932363	0.513888	54.3961	0.367279	40.3345
26,389	180.00	20.00	17.60	1.136364	0.539743	5.450199	0.521193	55.0564	0.369736	40.5823
26,390	180.00	20.00	17.80	1.123596	0.512315	5.000239	0.528526	55.7153	0.372158	40.8263
26,391	180.00	20.00	18.00	1.111111	0.484322	4.579285	0.535889	56.3727	0.374546	41.0665
26,392	180.00	20.00	18.20	1.098901	0.455613	4.184352	0.543280	57.0287	0.376901	41.3030
26,393	180.00	20.00	18.40	1.086957	0.425998	3.812606	0.550699	57.6830	0.379224	41.5358
26,394	180.00	20.00	18.60	1.075269	0.395225	3.461274	0.558145	58.3357	0.381514	41.7651
26,395	180.00	20.00	18.80	1.063830	0.362952	3.127537	0.565619	58.9866	0.383773	41.9909
26,396	180.00	20.00	19.00	1.052632	0.328684	2.808334	0.573119	59.6357	0.386001	42.2132
26,397	180.00	20.00	19.20	1.041667	0.291667	2.500018	0.580647	60.2829	0.388198	42.4322
26,398	180.00	20.00	19.40	1.030928	0.250624	2.197581	0.588200	60.9281	0.390366	42.6480
26,399	180.00	20.00	19.60	1.020408	0.203059	1.892555	0.595780	61.5713	0.392505	42.8605
26,400	180.00	20.00	19.80	1.010101	0.142492	1.564635	0.603385	62.2123	0.394615	43.0699

* Due to limited available space, only a small fraction of the whole table is displayed in the paper.

Numerical solving of the transcendental Equation (25) was conducted by employing Python's SciPy library "fsolve" function which is a wrapper around MINPACK's HYBRD and HYBRJ algorithms. HYBRD and HYBRJ are essentially the same, but HYBRD uses forward-difference approximation to compute the jacobian whereas HYBRJ requires the user to provide the jacobian. The purpose of HYBRD is to find a zero of a system of N nonlinear functions in N variables by a modification of the Powell hybrid method [33]. The user must provide a subroutine which calculates the functions.

3.3. Regression Model Substituting Numerical Solution of Transcedental Equation

Although the presented method for numerical solutions of a transcendental equation returns accurate values of the substitution *t* and consequently the precise vehicle position where the maximum transient offtracking is reached, its practical application is inefficient and requires advanced mathematical and programming skills. To address this issue, it is necessary to create a more efficient and simplified calculation procedure which is able to instantly return the required parameters determining the maximum transient offtracking position with the desired accuracy. Moreover, a newly designed calculation tool should eliminate the need to perform any additional vehicle movement simulation or swept path analysis in order to determine the critical vehicle position in an active transient offtracking state.

Regarding a relatively big dataset of generated input parameters and corresponding calculation results, the selection of an appropriate regression model which can predict the substitution *t* with the desired level of accuracy turned out to be the most practical solution. Several widely used nonlinear regression models were tested and compared by applying available Python functions. The benchmark for the desired level of accuracy of the tested regression models applied for the prediction of the steering angle β_d is set as 1/10 of the 1° angle, or in decimal form 0.10°. This means that the maximum error allowed or root mean square error (RMSE), when predicting the value of the substitution *t* by using the tested regression model is as follows:

$$RMSE_t = tg\left(\frac{\beta_d}{2}\right) = tg\left(\frac{0.10°}{2}\right) = 0.000873 \tag{29}$$

But, for engineers and practitioners it is probably more important what the previously set benchmark for the maximum RMSE value represents in a geometrical sense. Bearing in mind that the maximum allowed single-bus length is around 14.5 m, a 0.1° error in the predicting steering angle β_d, with a fourth-degree polynomial regression function, guarantees a 0.025 m lateral accuracy (tan (0.1°)·14.5 m = 0.025 m). Polynomial regression of the third degree produces a 0.05 m lateral accuracy, while second-degree polynomial regression results in errors exceeding 0.10 m. The single bus was selected as an appropriate design vehicle to calculate the lateral positioning error due to its long wheelbase.

In Table 2, the results of testing various nonlinear regression models and their corresponding RMSE metrics are listed.

Table 2. Tested nonlinear regression model for the prediction of substitution *t* values.

Nonlinear Regression Model Type	RMSE
Polynomial Regression (4th degree)	0.000496
Ridge Regression	0.002261
Lasso Regression	0.073637
Elastic Net Regression	0.073637
Decision Tree Regression	0.002843
Random Forest Regression	0.000995
Support Vector Regression—SVR	0.051933
Gradient Boosting Regression	0.001854
K Neighbors Regression	0.001480
AdaBoost Regression	0.009943

Evaluation of the compared regression models was not performed by using the whole set of input data (26,400 combinations in total)—80% of the combinations from the input dataset were used to train the models, while the remaining 20% were used for testing. This specific ratio for the input dataset split used later for the model training and testing is recommended by advanced Python users [34].

As can be seen in Table 2, only polynomial fourth-degree regression fulfills the set benchmark for the maximum RMSE value. Even when the whole set of the input data was considered, the obtained RMSE value for the polynomial fourth-degree regression is 0.000508, which is still the best in comparison to the other tested regression models. In addition to the desired value of RMSE, the coefficient of determination of the R-squared value (R^2) for the selected polynomial regression model is $R^2 = 0.99988$. Despite the R^2 not considering overfitting, the achieved R^2 value is very close to 1. Before the fourth-degree polynomial regression model was adopted as an optimal solution, second- and third-degree polynomial regression models were also tested, but their RMSE values, as well as their lateral positioning errors, were considerably higher than the previously established benchmark. In addition, as displayed in the Table 3, the obtained R^2 values for the second and third polynomial regression models were also very close to 1, but their RMSE metrics could not meet the desired level of accuracy.

Table 3. Lateral positioning error, RMSE, and R^2 values for polynomial regression of various orders.

Degree of Polynomial Regression Model	Lateral Positioning Error [m]	RMSE	R^2
2nd-degree polynomial regression	>0.100	0.002453	0.99904
3rd-degree polynomial regression	0.050	0.001754	0.99944
4th-degree polynomial regression	0.025	0.000496	0.99988

The relationship between the dependent variable, i.e., the substitution *t*, and the independent variables representing the turn angles θ_S and R/d ratio in the modeled polynomial regression function looks as follows:

$$
\begin{aligned}
t = \quad & -0.044417+0.044078\cdot\left(\tfrac{R}{d}\right)+0.004485\cdot\theta_s+(-0.010769)\cdot\left(\tfrac{R}{d}\right)^2+(-0.001131)\cdot\left(\tfrac{R}{d}\right)\cdot\theta_s+ \\
& (-6.53\cdot10^{-6})\cdot\theta_s^2+(-6.78\cdot10^{-5})\cdot\left(\tfrac{R}{d}\right)^3+0.000310\cdot\left(\tfrac{R}{d}\right)^2\cdot\theta_s+(-6.35\cdot10^{-6})\cdot\left(\tfrac{R}{d}\right)\cdot\theta_s^2+ \\
& 2.61\cdot10^{-8}\cdot\theta_s^3+0.000215\cdot\left(\tfrac{R}{d}\right)^4+(-3.68\cdot10^{-5})\cdot\left(\tfrac{R}{d}\right)^3\cdot\theta_s+(7.34\cdot10^{-7})\cdot\left(\tfrac{R}{d}\right)^2\cdot\theta_s^2+ \\
& 9.36\cdot10^{-9}\cdot\left(\tfrac{R}{d}\right)\cdot\theta_s^3+(-5.80\cdot10^{-11})\cdot\theta_s^4
\end{aligned}
\tag{30}
$$

The formula is rather a complex one, but it could be processed easily on a handheld computer, even the one installed in an autonomous vehicle. Though perhaps impractical for common use and not concurrent with vehicle movement simulation software, the mathematical solution developed herein could easily be used to guide the vehicle safely through the sharp turn. With the substitution t finally retrieved, the critical angle β_d and critical distance F_d could be calculated easily ($\beta_d = 2\cdot arctg(t)$ and $F_d = (d - R\cdot sin\beta_d)/cos\beta_d$). Three-dimensional plots and graphs illustrating the relationship amongst the substitution t and the independent variables θ_S and R/d are displayed in Figure 8.
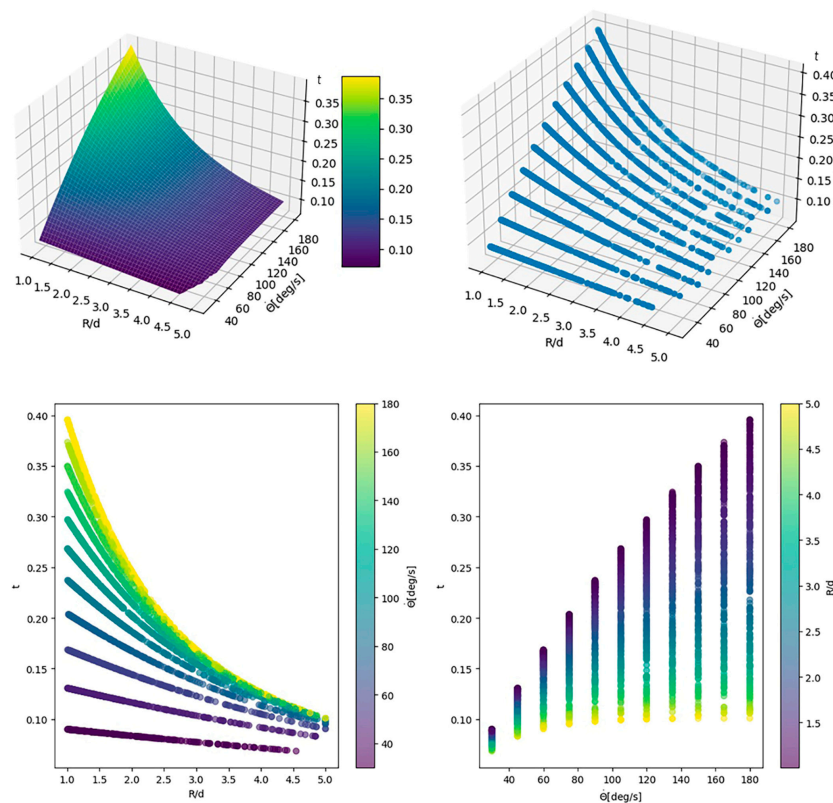
Figure 8. Graphical interpretation of relationship amongst the substitution t, turn angle θ_S, and R/d ratio.

4. Evaluation of the Adopted Regression Model and Discussion

In this section, an evaluation of the adopted regression model is performed and some practical aspects of its application are discussed. The simplest method of evaluation assumes the use of existing Python tools and plotting substitution t values, retrieved using numerical methods, against the values coming from the polynomial regression model. An example of such a diagram, covering the whole set of generated input data, is shown in Figure 9.

Figure 9. Graphical interpretation of the relationship between the substitution *t* values obtained from numerical calculation and the polynomial regression model.

It is evident from the diagram in Figure 9 that the polynomial regression function fits the numerically calculated values of the substitution *t* very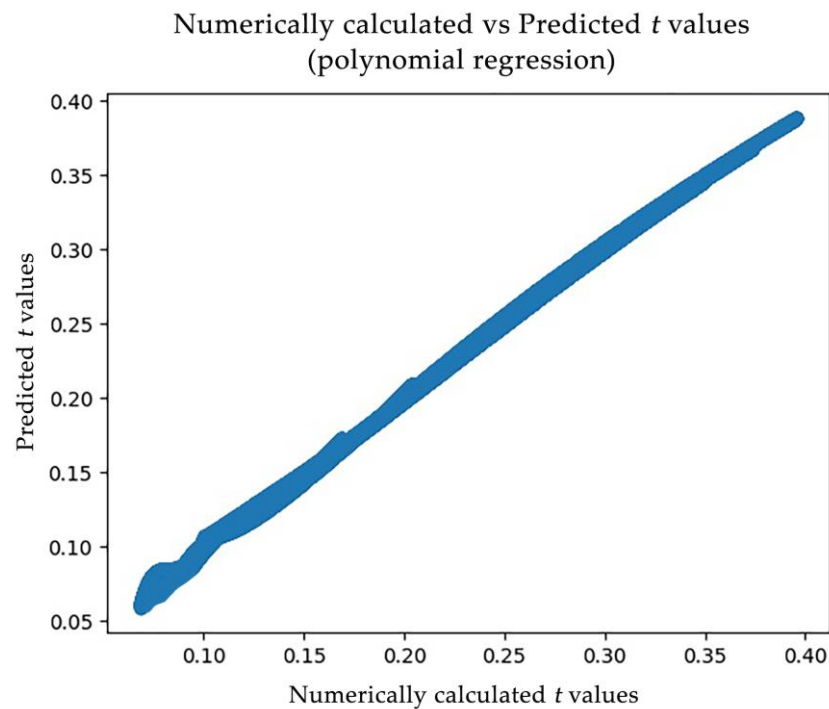 well. A certain discrepancy occurs for the substitution *t* values of less than 0.10, which corresponds to turn angles θ_S smaller than 40°.

To evaluate the potential limitations and pre-suppositions for its use, robustness analyses of the adopted polynomial regression model were conducted. Standard methods and their corresponding procedures, briefly described in Table 4, were applied to test the robustness of the established fourth-degree polynomial regression model.

Table 4. Overview of standard methods to test robustness of a regression model.

No	Methods	Brief Description of Steps to Test the Robustness of the Selected Method
1	K-Fold Cross-Validation	The procedure has a single parameter called k that refers to the number of groups that a given data sample is to be split into. As such, the procedure is often called k-fold cross-validation.
2	Repeated Train/Test Splits	Perform multiple train/test splits with different random seeds and evaluate the model on each split. Calculate and compare the performance metrics (e.g., R^2, RMSE) across these splits.
3	Robustness to Noise	Add different levels of noise to the input features and observe changes in performance metrics. For example, Gaussian noise can be added to analyzed features to see how the model's predictions and accuracy are affected.
4	Outlier Analysis	Introduce synthetic outliers into the dataset and evaluate the model's robustness by observing changes in performance metrics.
5	Generalization to Unseen Data	If researchers have access to an external dataset that was not used in training, they can evaluate the model on this dataset to check its generalization capabilities.
6	Stress Testing with Extreme Values	Test the regression model with extreme or edge-case values for input features to evaluate how it handles these unusual cases.

K-fold cross-validation was used for the RMSE and R^2 metrics' robustness testing. Herein, the parameter k was equal to 5, which means that the sample dataset was divided into five parts that were (roughly) equal in size. The k-fold cross-validation results are listed below:

- Cross-validation RMSE scores: [0.00050482 0.00051121 0.00050779 0.00050810 0.00052693];
- Cross-validation mean RMSE score: 0.00051177;
- Cross-validation R^2 Scores: [0.99987991 0.99988177 0.9998805 0.99987864 0.99987698];
- Cross-validation mean R^2 score: 0.99987956.

The produced cross-validation RMSE scores and the corresponding mean show that there is no RMSE value above the established benchmark for the desired level of accuracy (Equation (29)). Also, the obtained cross-validation R^2 scores and their mean negligibly differ from the R^2 value which was initially achieved for the whole generated dataset.

The methods "repeated train/test Splits, robustness to noise, outlier analysis, and generalization to unseen data" cannot be directly implemented because polynomial regression function was established by using the whole dataset. In addition, the used dataset with different combinations of parameters R, d and θ was artificially created, while the previously listed methods, particularly robustness to noise and outlier analysis, are more suitable for the robustness analysis of experimentally collected data, i.e., data acquired from measurements in the field. Generalization to unseen data requires the introduction of an external dataset that was not used in model training, which is not relevant in this case—because predetermined combinations of the key input parameters R, d, and θ were used to generate the whole dataset.

The stress testing with extreme values method gave the following results:

- MSE on the high-value subset (HVS) range: 2.757111×10^{-7};
- RMSE on the HVS range: 0.000403;
- MSE on the low-value subset (LVS) range: 6.017358×10^{-7};
- RMSE on the LVS range: 0.000595.

HVS includes predicted values of substitution t in the range: $t > \text{MDN}_t$;
LVS includes predicted values of substitution t in the range: $t \leq \text{MDN}_t$.

It can be seen that higher mean square error (MSE) and RMSE values were obtained below the median (MDN) of predicted substitution t values, which is MDNt = 0.188780. MDNt closely matches to the combination of the turn angle θ of 75° and the R/d ratio of 1.40845. This means that the adopted regression model has a slightly lower accuracy for turn angles θ smaller than 75° and R/d ratios below 1.408451 or $d = 0.71 \cdot R$.

Robustness analyses of the fourth-degree polynomial regression model revealed new pre-suppositions for its use. In addition to the precondition $R > d$, originally imposed by the ICAO, and the numerically calculated possible range for the substitution t values $0 < t < 1$ (Equation (28)), robustness analyses pointed out that the regression model has a negligibly lower prediction accuracy for the turn angles of $\theta < 75°$ and R/d ratios in the range of $R/d < 1.408451$.

The accuracy of the adopted regression model was thoroughly evaluated by comparing substitution t values calculated both numerically and by the fourth-degree polynomial regression function (29). In addition to the substitution t values, corresponding steering angles β_d and distances $F_{OT_{max}}$ determining the vehicle maximum transient offtracking positions were calculated and mutually compared. As expected, the biggest absolute differences between the parameters β_d and $F_{OT_{max}}$ calculated by the two compared methods appear only in a limited number of cases for the combinations of input parameters at the beginning of the generated input dataset. These critical combinations of input parameters refer to the ones with the smaller turn angles θ_S, usually less than 35°, which is in accordance with the previous findings acquired from the diagram displayed in Figure 9 and robustness analyses.

Moreover, the results of the calculation methods' comparison displayed in Table 5 should be discussed from the road designers' perspective as well. Although the 0.20 m difference between the compared values F_{OTmax} at first seems like a serious error in the prediction of the regression model, it should be highlighted that it is actually an error in determining the position of the vehicle's datum point in the "longitudinal sense". In contrast to this, the observed error in the "lateral sense" is far smaller, as can be seen in Figure 10.

Table 5. Comparison of the values of t, β_d, and F_{OTmax} calculated numerically and by the regression model.

No *	Input Parameters			Numerical Solution			Regression Model			Abs. Differences	
	θ_S [°]	R/d	β_{max} [°]	t_N	β_{d-N} [°]	$F_{OTmax-N}$	t_R	β_{d-R} [°]	$F_{OTmax-R}$ [m]	$\Delta\beta_d$ [°]	ΔF_{OTmax} [m]
1	30.00	5.000000	10.6633	0.066106	7.5642	0.690	0.073171	8.3699	0.487	0.8057	0.203
2	30.00	4.761905	11.0811	0.067365	7.7078	0.766	0.072593	8.3039	0.609	0.5962	0.157
3	30.00	4.545455	11.4848	0.068529	7.8406	0.844	0.070955	8.1172	0.767	0.2767	0.077
4	30.00	4.347826	11.8748	0.069609	7.9637	0.923	0.070269	8.0390	0.902	0.0753	0.022
5	30.00	4.166667	12.2514	0.070612	8.0782	1.005	0.070210	8.0323	1.018	0.0459	0.014
6	30.00	4.000000	12.6151	0.071547	8.1848	1.087	0.070559	8.0721	1.122	0.1127	0.035
7	30.00	3.846154	12.9663	0.072420	8.2843	1.171	0.071166	8.1413	1.217	0.1430	0.045
8	30.00	3.703704	13.3054	0.073236	8.3773	1.256	0.071928	8.2282	1.305	0.1491	0.049
9	30.00	3.571429	13.6330	0.074001	8.4645	1.343	0.072777	8.3249	1.389	0.1396	0.047
10	30.00	3.448276	13.9493	0.074720	8.5464	1.430	0.073663	8.4260	1.471	0.1204	0.041
11	30.00	3.333333	14.2550	0.075395	8.6233	1.518	0.074557	8.5278	1.551	0.0955	0.034
12	30.00	3.225806	14.5504	0.076031	8.6958	1.607	0.075436	8.6280	1.631	0.0678	0.024
13	30.00	3.125000	14.8360	0.076632	8.7642	1.696	0.076287	8.7249	1.711	0.0393	0.014
14	30.00	3.030303	15.1121	0.077199	8.8288	1.786	0.077100	8.8176	1.791	0.0112	0.004
15	30.00	2.941176	15.3792	0.077736	8.8900	1.877	0.077872	8.9055	1.871	0.0156	0.006
16	30.00	2.857143	15.6376	0.078244	8.9479	1.969	0.078600	8.9884	1.953	0.0405	0.016
17	30.00	2.777778	15.8876	0.078727	9.0029	2.061	0.079283	9.0662	2.035	0.0633	0.025
•	•	•	•	•	•	•	•	•	•	•	•
•	•	•	•	•	•	•	•	•	•	•	•
•	•	•	•	•	•	•	•	•	•	•	•
26,383	180.00	1.219512	51.0779	0.354454	39.0342	4.898	0.354516	39.0405	4.895	0.0063	0.003
26,384	180.00	1.204819	51.7435	0.357094	39.3026	5.081	0.357041	39.2973	5.083	0.0053	0.002
26,385	180.00	1.190476	52.4083	0.359695	39.5668	5.267	0.359525	39.5496	5.275	0.0172	0.008
26,386	180.00	1.176471	53.0720	0.362259	39.8268	5.457	0.361969	39.7974	5.470	0.0294	0.014
26,387	180.00	1.162791	53.7347	0.364787	40.0826	5.649	0.364375	40.0409	5.668	0.0417	0.019
26,388	180.00	1.149425	54.3961	0.367279	40.3345	5.844	0.366742	40.2802	5.870	0.0543	0.025
26,389	180.00	1.136364	55.0564	0.369736	40.5823	6.043	0.369071	40.5153	6.074	0.0670	0.032
26,390	180.00	1.123596	55.7153	0.372158	40.8263	6.244	0.371364	40.7464	6.282	0.0799	0.038
26,391	180.00	1.111111	56.3727	0.374546	41.0665	6.448	0.373621	40.9735	6.492	0.0930	0.045
26,392	180.00	1.098901	57.0287	0.376901	41.3030	6.655	0.375843	41.1968	6.706	0.1062	0.051
26,393	180.00	1.086957	57.6830	0.379224	41.5358	6.864	0.378030	41.4162	6.922	0.1196	0.058
26,394	180.00	1.075269	58.3357	0.381514	41.7651	7.077	0.380184	41.6320	7.142	0.1331	0.065
26,395	180.00	1.063830	58.9866	0.383773	41.9909	7.292	0.382305	41.8442	7.364	0.1466	0.072
26,396	180.00	1.052632	59.6357	0.386001	42.2132	7.510	0.384394	42.0529	7.589	0.1603	0.079
26,397	180.00	1.041667	60.2829	0.388198	42.4322	7.730	0.386451	42.2581	7.817	0.1741	0.087
26,398	180.00	1.030928	60.9281	0.390366	42.6480	7.954	0.388477	42.4600	8.048	0.1880	0.094
26,399	180.00	1.020408	61.5713	0.392505	42.8605	8.180	0.390473	42.6586	8.281	0.2019	0.102
26,400	180.00	1.010101	62.2123	0.394615	43.0699	8.408	0.392439	42.8540	8.517	0.2159	0.109

* Due to limited available space, only a small fraction of the whole table is displayed in the paper.

To more practically explain the minor importance of errors in the "longitudinal sense" when determining F_{OTmax} distances on the overall accuracy of the maximum transient offtracking calculation, one of the situations with an unfavorable (critical) combination of input parameters (R, d, and θ_S) is presented in Figure 10. The selected vehicle with a datum length d = 5.00 m negotiates a circular curve with a turn angle of 30° and a radius R = 20 m. The required parameters F_{OTmax} and β_d, determining the maximum transient offtracking position of the vehicle, are calculated numerically.
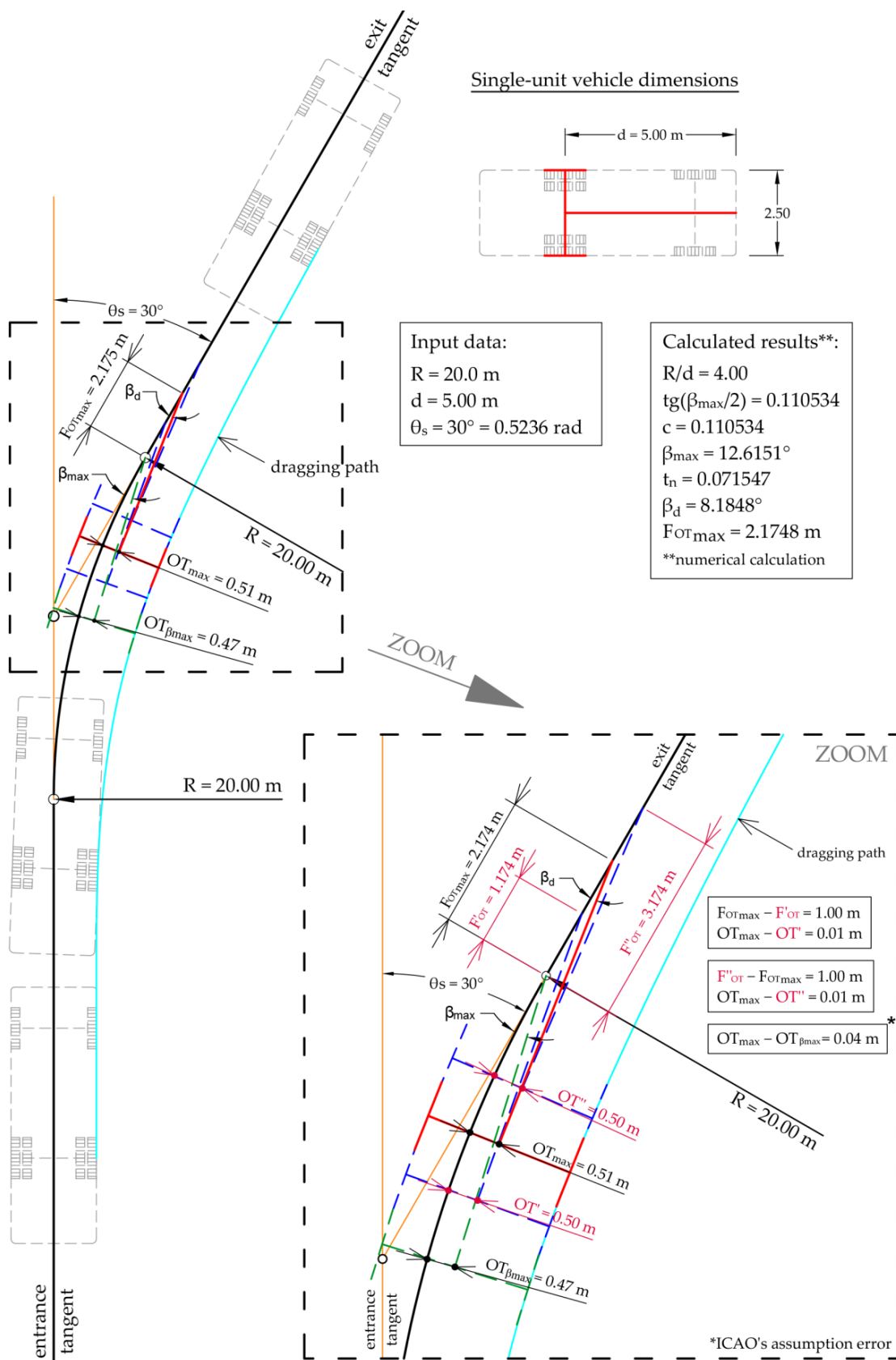
Figure 10. The influence of the magnitude of error in the "longitudinal sense" (when calculating $F_{OT_{max}}$) on the accuracy of the maximum transient offtracking vehicle position.

Figure 10 proves that the lateral offset (transient offtracking) varies slightly whether the vehicles datum point is moved back or forth along the exit tangent, in relation to the point where the actual maximum transient offtracking is reached. Of course, the movement of the point concerned should stay within reasonable limits (1.0 m in Figure 10). Negligible differences between the pairs of lengths OT_{max} and OT', and OT_{max} and OT'', confirm that. From the presented example, it is clear that the maximum error of $\Delta F_{OT_{max}} = 0.203$ m when calculating $F_{OT_{max}}$ distances using the derived polynomial regression function, in terms of practical engineering applications, has a negligible impact on the overall computation accuracy of the maximum transient offtracking position.

Now, it is important to notice that the difference between the maximum transient offtracking value OT_{max} and the offtracking $OT_{\beta max}$, calculated in the position where the maximum steering angle β_{max} is reached (the exact end of the arc) is 0.04 m. Though some safety margins must always be observed, the typical accuracy of construction works in plan projection must be within 1 cm. And as for aircraft negotiating taxiway turns, the error becomes much higher, compromising not specific ICAO formulas but the entire calculation procedure. The formulas recommended by the ICAO are absolutely correct, but the assumption that the maximum offtracking is reached when the aircraft datum point reaches the end of an arc is absolutely incorrect. In the common taxiway fillet case, when a Boeing 747–100 negotiates a $\theta_S = 90°$, $R = 50.00$ m curve, the error increases up to 0.30 m. In the same turn, the Airbus A380 produces a 0.75 m error. In a less common situation, the A380 negotiating a $\theta_S = 45°$, $R = 50.00$ m turn, the error is 2.79 m. With θ_S decreasing to $30°$, the error exceeds 4.3 m! There are even some rare θ_S, R combinations producing errors exceeding 6.0 m!

5. Conclusions

The calculation method presented herein offers a unique and practical solution for the calculation of the maximum transient offtracking of a single-unit vehicle when negotiating circular curves. It uses well-proven mathematical formulas from the ICAO mathematical model for the derivation of only one transcendental equation which precisely determines the maximum transient offtracking position of the vehicle. Complicated numerical methods for solving this type of equation were substituted by a relatively simple polynomial regression function capable to predict the maximum transient offtracking position with the desired level of accuracy. In this manner, computationally demanding numerical methods for transcendental equation solving are successfully compensated with a more practical and efficient calculation method. The accuracy of the presented regression model was assessed on the whole set of input data parameters, including all combinations of R/d ratios and θ_S turn angles. The largest discrepancies in relation to the numerical calculations appear for turn angles θ_S smaller than $35°$, but the magnitude of these discrepancies negligibly affects the reliability and overall accuracy of the developed regression model. Robustness analyses of the fourth-degree polynomial regression model revealed that the regression model has a negligibly lower prediction accuracy for the combination of input parameters covering turn angles $\theta < 75°$ and R/d ratios in the range $R/d < 1.408451$.

Though the polynomial regression function seems too long at first sight, its main advantage is the almost instant calculation of the maximum transient offtracking position. Minimal effort and an ordinary pocket calculator are enough to calculate maximum transient offtracking position for the specified input parameters R, d, and θ_S. All previously published mathematical models and, in particular, the currently available software tools for vehicle swept path analyses require more time and engineering skills to achieve the same results. Additionally, the method retrieves the maximum transient offtracking from the three input parameters (R, d, and θ_S), skipping the need for CAD-like steering path construction (as an input) and swept path generation (as an output).

It is demonstrated and proved that the maximum transient offtracking is not achieved when the vehicle's datum point reaches the end of circular arc (assumption in ICAO's design manual), but some distance beyond. What is more important, the error caused by this ICAO's assumption can significantly affect the accuracy of fillet design at airports.

By applying the regression model proposed herein, it is possible to calculate the maximum transient offtracking only when the vehicle negotiates simple circular curves. For other steering alignment configurations, which include more complex horizontal curve types, i.e., transition and revers curves, this method cannot be used. Currently, the proposed regression model can be applied for the maximum transient offtracking calculation of a single-unit vehicle and not for articulated or multi-unit vehicle combinations. These flaws have already been considered by the authors of the paper and new mathematical models which tackle these issues are already under development.

Author Contributions: Conceptualization, V.I. and D.G.; formal analysis, M.L.; investigation, S.F., F.T. and S.V.; methodology, V.I. and D.G.; software, M.L.; supervision, V.I. and D.G.; visualization, F.T., S.V. and N.M.; writing—original draft, V.I., D.G. and S.F.; writing—review and editing, V.I. and M.L. All authors have read and agreed to the published version of the manuscript.

Institutional Review Board Statement: Not applicable.

Informed Consent Statement: Not applicable.

Data Availability Statement: Data is contained within the article.

Abbreviations

Abbreviation	Description
θ_s	turn angle—in [°]
d	aircraft (vehicle) datum length—in [m]
R	circular curve radii—in [m]
S	aircraft datum point
U	aircraft main undercarriage center
β	steering angle—in [°]
X	R/d ratio
β_{max}	maximum steering angle—in [°]
F	distance that aircraft datum point (S) covered along arc exit tangent—in [m]
OT_{max}	maximum transient offtracking—in [m]
F_{OTmax}	distance that aircraft datum point (S) covered along arc exit tangent in maximum transient offtracking position—in [m]
w	vehicle track width—in [m]
β_d	steering angle between the longitudinal aircraft axis and exit tangent in maximum transient offtracking position— in [°]
c	constant
t	substitution (independent variable)
$RMSE$	root mean square error
R^2	coefficient of determination (R-squared value)
MSE	mean square error
MDN_t	median of predicted substitution t values
HVS	high value subset
LVS	low value subset
t_N	substitution t calculated numerically
t_R	substitution t calculated by polynomial regression function

Abbreviation	Description
$\beta_{d\text{-}N}$	steering angle β_d obtained from the substitution t numerically calculated— in [°]
$\beta_{d\text{-}R}$	steering angle β_d obtained from the substitution t calculated by adopted polynomial regression function— in [°]
$F_{OTmax\text{-}N}$	distance F_{OTmax} obtained from numerically calculated substitution t and steering angle $\beta_{d\text{-}N}$—in [m]
$F_{OTmax\text{-}R}$	distance F_{OTmax} obtained from the substitution t and steering angle $\beta_{d\text{-}R}$ calculated by polynomial regression function—in [m]
$\Delta\beta_d$	absolute differences between previously calculated steering angles $\beta_{d\text{-}N}$ and $\beta_{d\text{-}R}$—in [°]
ΔF_{OTmax}	absolute differences between previously calculated distances $F_{OTmax\text{-}N}$ and $F_{OTmax\text{-}R}$—in [m]
$OT_{\beta max}$	transient offtracking calculated in the position where the maximum steering angle β_{max} is reached—in [m]

References

1. AASHTO. Elements of design—Horizontal alignment. In *The Green Book—A Policy on Geometric Design of Highways and Streets*, 7th ed.; American Association of State Highway and Transportation Officials—AASHTO: Washington, DC, USA, 2018; pp. 90–96.
2. Jindra, F. Off-Tracking of Tractor-Trailer Combinations. In *Automobile Engineer*; SAE International: London, UK, 1963; pp. 96–101.
3. Sayers, M.W. *Vehicle Offtracking Models*; Transportation Research Record 1052; Transportation Research Board: Washington, DC, USA, 1986; pp. 53–62.
4. Choi, J.; Lee, S.; Baek, J.; Kang, W. Offtracking Model on Horizontal Curve Sections. *Proc. East. Asia Soc. Transp. Stud.* **2001**, *3*, 341–353.
5. National Academies of Sciences, Engineering, and Medicine. *NCHRP Report 505: Review of Truck Characteristics as Factors in Roadway Design*; The National Academies Press: Washington, DC, USA, 2003; pp. 39–44. [CrossRef]
6. Erkert, T.W.; Sessions, J.; Layton, R.D. A Method for Determining Offtracking of Multiple Unit Vehicle Combinations. *J. For. Eng.* **1989**, *1*, 9–16. [CrossRef]
7. Woodrooffe, J.H.F.; Smith, C.A.M.; Morisset, L.E. A Generalized Solution of Non-Steady State Vehicle Off Tracking in Constant Radius Curves. In Proceedings of the 3rd International Pacific Conference on Automotive Engineering: Motor Vehicle Technology: Mobility for prosperity, Jakarta, Indonesia, 11–14 November 1985. [CrossRef]
8. WHI. *Offtracking Characteristics of Trucks and Truck Combinations*; Research Committee Report No. 3; Western Highway Institute: San Bruno, CA, USA, 1970; pp. 7–45.
9. SAE. *Turning Ability and Off Tracking—Motor Vehicles*; SAE Recommended Practice, J695_201106; Society of Automobile Engineers—SAE International: Warrendale, PA, USA, 2011; p. 13. [CrossRef]
10. SAE. *Turning Ability and Off Tracking—Motor Vehicles*; SAE Recommended Practice, J695_202401; Society of Automobile Engineers—SAE International: Warrendale, PA, USA, 2024; p. 12. [CrossRef]
11. ICAO. Appendix 1—Fillet design. In *Aerodrome Design Manual—Part 2: Taxiways, Aprons and Holding Bays*, 5th ed.; International Civil Aviation Organization: Montreal, QC, Canada, 2020; pp. 97–143.
12. Yao, Q.; Tian, Y.; Wang, Q.; Wang, S. Control Strategies on Path Tracking for Autonomous Vehicle: State of the Art and Future Challenges. *IEEE Access* **2020**, *8*, 161211–161222. [CrossRef]
13. Othman, K. Impact of Autonomous Vehicles on the Physical Infrastructure: Changes and Challenges. *Designs* **2021**, *5*, 40. [CrossRef]
14. Kebbati, Y.; Ait-Oufroukh, N.; Ichalal, D.; Vigneron, V. Lateral control for autonomous wheeled vehicles: A technical review. *Asian J. Control* **2023**, *25*, 2539–2563. [CrossRef]
15. Jawahar, A.; Palla, L. Lateral Control of Heavy Vehicles. Master's Thesis, KTH Royal Institute of Technology, School of Engineering Sciences, Stockholm, Sweden, 2023.
16. Shaju, A.; Southward, S.; Ahmadian, M. Enhancing Autonomous Vehicle Navigation with a Clothoid-Based Lateral Controller. *Appl. Sci.* **2024**, *14*, 1817. [CrossRef]
17. Sayers, M.W. Symbolic Computer Methods to Automatically Formulate Vehicle Simulation Codes. Doctoral Thesis, The University of Michigan Transportation Research Institute, Ann Arbor, MI, USA, 1990.
18. Sayers, M.W. Exact Equations for Tractrix Curves Associated with Vehicle Offtracking. *Veh. Syst. Dyn.* **1991**, *20*, 297–308. [CrossRef]
19. Garlick, G.S.; Kanga, D.N.; Miller, G.G. Vehicle Offtracking: A Globally Stable Solution. *ITE J.* **1993**, *63*, 17–21.
20. Wang, Y.; Linnett, J.A. Vehicle Kinematics and Its Application to Highway Design. *J. Transp. Eng.-ASCE* **1995**, *121*, 63–74. [CrossRef]
21. Dragčević, V. Numerical Model of Motion of Road Vehicles. Doctoral Thesis, The University of Zagreb, Faculty of Civil Engineering, Zagreb, Croatia, 1999.
22. Prince, G.E.; Dubois, S.P. Mathematical Models for Motion of the Rear Ends of Vehicles. *Math. Comput. Model.* **2009**, *49*, 2049–2060. [CrossRef]

23. Cheng, J.F.; Huang, H.C. Effects of Roadway Geometric Features on Low- Speed Turning Maneuvers of Large Vehicles. *Int. J. Pavement Res. Technol.* **2011**, *4*, 373–383.

24. Autodesk. Vehicle Tracking: Swept Path Analysis and Design Software. Available online: https://www.autodesk.com/products/vehicle-tracking/overview (accessed on 11 April 2024).

25. Transoft Solutions. AutoTURN: Vehicle Simulation Software. Available online: https://www.transoftsolutions.com/emea/civil-and-transportation/software/swept-path-analysis/autoturn/ (accessed on 11 April 2024).

26. Ilić, V. Analytical Method for Critical Vehicle Swept Path Testing and Intersection Layout Elements Calculation. Doctoral Thesis, The University of Belgrade, Faculty of Civil Engineering, Belgrade, Serbia, 2019.

27. Lawrence, G.J. A mathematical Model for the Low-Speed Offtracking of Articulated Vehicles That Includes Tire Mechanics. Master's Thesis, The University of Calgary, Department of Mechanical Engineering, Calgary, AB, Canada, 1987.

28. Dragčević, V.; Korlaet, Ž.; Stančerić, I. Methods for Setting Road Vehicle Movements Trajectories. *Balt. J. Road Bridge Eng.* **2008**, *3*, 57–64. [CrossRef]

29. Stančerić, I.; Korlaet, Ž.; Dragčević, V. New design procedure for four-leg channelized intersections. *Građevinar* **2017**, *69*, 257–266. [CrossRef]

30. Forschungsgessellschaft für Straßen und Verkehrswesen (FGSV). *Richtlinien für die Anlage von Landstrassen—RAL, Abschnitt 6: Knotenpunkte, Unterabschnitt 6.4: Knotenpunktelemente—Rechtsabbiegen*; Forschungsgessellschaft für Straßen und Verkehrswesen (FGSV): Köln, Germany, 2012.

31. CGS Labs. Autopath: Swept Path Analysis and Vehicle Turning Simulation Software. Available online: https://cgs-labs.com/autopath/ (accessed on 13 April 2024).

32. Luck, R.; Zdaniuk, G.J.; Cho, H. An Efficient Method to Find Solutions for Transcendental Equations with Several Roots. *Int. J. Eng. Math.* **2015**, *2015*, 523043. [CrossRef]

33. HYBRD. Documentation for MINPACK Subroutine HYBRD. Available online: https://www.math.utah.edu/software/minpack/minpack/hybrd.html (accessed on 26 April 2024).

34. Real Python. Advanced Python Tutorials. Available online: https://realpython.com/tutorials/advanced/ (accessed on 30 April 2024).